Effect of Pre-stressing on the Growth Direction of Surface Cracks in Ultrafine Grained Copper

K. Kamil[1], M. Goto[1*], S. Z. Han[2], K. Euh[2], T. Yakushiji[3] and Y. Tatsukawa[1]

[1] Department of Mechanical Engineering, Oita University, Oita, 870-1192, Japan.
[*]masagoto@oita-u.ac.jp
[2] Korea Institute of Materials Science, Changwon, Republic of Korea.
[3] Department of Mechanical Eng., Oita National College of Technology, Oita, Japan.

ABSTRACT. *Crack growth direction of ultrafine grained copper under constant stressing depended on the magnitude of the applied stress amplitude, perpendicular to the loading axis at low stresses, and inclined at 45° to the loading axis at high stresses. To clarify the different growth mechanisms between the high- and low-stress amplitudes, two-step fatigue stress tests were conducted. In the case of high-to-low block stressing, the 45° inclined growth direction under high stress changed to the perpendicular direction under subsequent low stress. In macroscale low-to-high block stressing, the crack growth direction before and after the stress change was nearly perpendicular to the loading axis. On a microscale, however, the degree of zigzag manner in the crack growth drastically increased after the stress change. The formation mechanism of the crack paths under high- and low-stress amplitudes and the effect of pre-stressing on subsequent crack growth direction were discussed from the viewpoints of the evolution of damaged areas around the crack tip.*

INTRODUCTION

Equal channel angular pressing (ECAP), has been currently used to obtain ultrafine grains (UFG), which are tenfold to hundredfold finer than those of conventional materials. These materials, generally, possess many unique properties such as high tensile strength, fairly large plasticity at low temperature, etc. [1]. These unique properties of UFG materials are due to unusual microstructure which is often regarded as 'non-equilibrium' states.

Until recently, most studies have focused on optimizing processing conditions, underlying microstructural mechanisms, attainable post-ECAP strength levels [1,2]. For envisaged structural applications of UFG metals, attention has been paid to fatigue performance such as cyclic properties, S-N characteristics, and formation of shear bands (SBs) [3-9]. Fatigue crack propagation has recently attracted great interest. On the surface of cyclically deformed UFG metals, SBs extend over a much larger distance than the UFG grain size that is usually formed [4,5]. In strain-controlled low-cycle fatigue (LCF) tests, SBs in the ZX-plane were oriented at 45° to the loading axis parallel

to the longitudinal axis of the pressed samples, while that in the XY-plane was nearly perpendicular to the loading axis (the ZX- and XY-plane: refer to Fig. 1) [10,11]. Fatigue cracks were initiated in and propagated along these SBs. No direct relationship was seen between SB formation and the oriented distribution of defects along the streamline plane due to shear direction in the ECAP [12]. The SBs appear on a ZX-plane at 45° to the loading direction mainly because it is the plane of maximum resolved shear stress [4].

In the high-cycle fatigue (HCF) regime, the growth behavior of millimeter-range cracks in UFG metals has been studied using compact tension (CT) [13-17], and single edge-notched specimens [18-20]. The crack growth direction of most of those specimens was nearly perpendicular to the loading axis; however, the positional relationship between the specimen faces and the XY-, YZ- and ZX-planes of the pressed samples was not clearly defined. Niendorf et al. [21] studied fatigue crack growth of UFG interstitial-free steel using the CT specimens. To allow for investigation of the role of the ECAP-induced microstructure, the faces of CT specimens were cut parallel to the XY-, YZ- or ZX-plane of the billets. They showed that both the ECAP processing route and the crack growth direction with respect to the extrusion direction dictate the crack growth behavior, and significant deviation from the expected crack growth normal direction to the loading axis was notable. This deviation was attributed to the presence of elongated structures that formed parallel to the material's plastic flow during ECAP processing. On the growth behavior of small cracks in HCF regime, Goto et al. monitored the growth behavior of surface cracks in round-bar UFG copper specimens and discussed the effect of microstructural inhomogeneity on growth path formation [22], a microstructure-related growth mechanism [23] and a small-crack growth law [24].

There are distinct differences in crack growth direction between LCF and HCF. However, little has been discussed about the physical background of different LCF and HCF growth behaviors. The objective of this paper is to investigate the crack growth mechanism at high and low cyclic stresses corresponding to LCF and HCF, respectively. In addition, the effect of pre-stressing on subsequent growth paths is discussed.

EXPERIMENTAL PROCEDURE

Material used was a pure oxygen-free copper (99.99 wt% Cu). Prior to the ECAP processing, the materials were annealed at 500 ˚C for 1 hr (average grain size: 100 μm). The post-annealed mechanical properties were 232 MPa tensile strength, 65% elongation, a Vickers hardness number equal to 63. Figure 1 shows a schematic of the ECAP die and direction of fatigue specimens relative of the pressing direction. The die had a 90° angle between intersecting channels. The inner and outer angles of the channel intersection in the ECAP die were 90° and 45°, respectively. Repetitive ECAP were accomplished through Bc route, in which the billet bar was rotated 90° around its longitudinal axis after each pressing. Eight time extrusions resulted in an equivalent

strain of about 7.8 [25] and the material properties changed to 438 MPa tensile strength, elongation 28% and 141 Vickers hardness number.

Fatigue specimens were machined from the ECAP-processed rods with their tensile axis lying parallel to the extrusion direction. The vertical plane parallel to extrusion direction is defined as ZX-plane, and the horizontal plane is XY-plane, as shown in Fig. 1. Figure 2 shows the shape and dimensions of fatigue specimens. The specimen had a shallow circumferential notch (20 mm notch radius and 0.25 mm notch depth) to localize damaged areas for successive observations of the surface. However, the fatigue strength reduction factor for this geometry was close to 1, so that the specimen can be considered as a plain specimen. Before testing, all fatigue specimens were electrolytically polished (~ 25 μm from the surface layer) prior to mechanical testing in order to remove any preparation affected surface layer. Polishing was carried out at 25 ˚C using an electrolyte consisting of 600 ml phosphoric acid, 300 ml distilled water and 100 ml sulfuric acid.

Prior to testing, a small blind hole (Fig.2: diameter and depth were both 0.1 mm) was drilled as a crack starter on the middle surfaces corresponding to ZX-plane as illustrated on Fig. 3. Fatigue tests were carried out at room temperature using a rotating

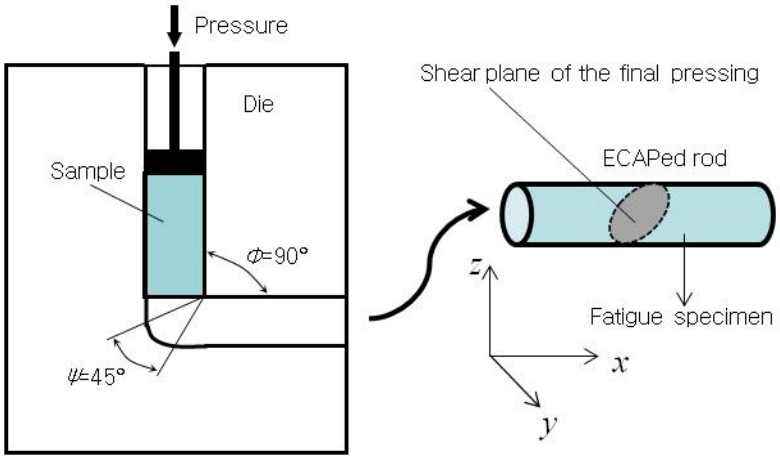

Figure 1. Equal channel angular pressing process overview and the definition of orientation of fatigue specimens relative to the final pressing direction.

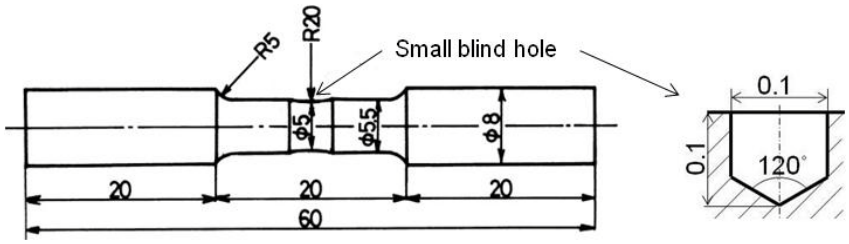

Figure 2. Dimensions of the fatigue smooth specimen and details of small blind hole (in mm).

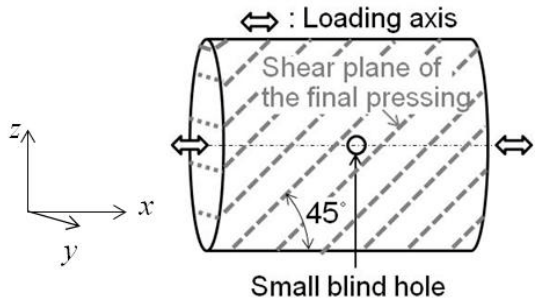

Figure 3. Drilling location of small blind hole.

bending fatigue machine operating at 50 Hz. Observations of fatigue damage on the specimen surface were performed using optical microscopy and scanning electron microscopy (SEM). The stress value referred to is that of the nominal stress amplitude, σ_a, at the minimum cross section. The crack length, l, was measured along the circumferential surface direction.

The cross-section perpendicular to the press direction was observed in the electron backscatter diffraction (EBSD) analyses. The specimens were ground using silicon carbide papers and polished with polycrystalline 3- and 1-μm diamond suspension. Final polishing was performed using a 0.04-μm colloidal silica suspension for 30–60 min. EBSD mappings were executed using a Tescan Mira II SEM incorporating an EDAX-TSL Hikari EBSD detector. Each hexagonally shaped pixel was 40 nm for the UFG copper samples. Orientation imaging microscopy (OIM) analysis software version 5.3 was used to analyze the orientation characteristics and misorientation distributions.

The degree of non-equilibrium state in the microstructures was measured using differential scanning calorimetry (DSC). The sample and reference were placed in thermally balanced alumina pans. The reference was made of the same copper as the sample but was in the fully annealed state. All of the experiments were performed using a nitrogen atmosphere in a DSC chamber during continuous heating with a ramp rate of 10°C/min up to 450°C.

RESULTS AND DISCUSSION

Figure 4 shows image quality (IQ) maps, inverse pole figure (IPF) maps, and grain boundary (GB) maps of the ECAPed samples. The cross-section perpendicular to the pressing direction was observed. The IQ maps represent the strain distribution; the bright and dark areas in the maps indicate less strained and highly strained regions with higher dislocation density, respectively. The high contrast arose from the variety of strain distributions in the GB regions, meaning there was a non-equilibrium state due to redundant defects. The difference in the heat flow (HF) values measured by DSC was 0.69 J/g for the UFG copper samples. The HF value here is not an absolute value of the stored energy in the microstructure, but it can be used for comparison with the degree of

stored energy generated by ECAP processing. The rationale for the HF measurement is that the HF of pure copper would be solely controlled by the generation and/or annihilation of dislocations and GBs during ECAP processing, unlike the other alloys that either had a precipitation hardening or a solid solution-hardening mechanism. As might be expected, the HF values of the fully annealed copper were almost zero. The large HF value for UFG copper indicated that the strain energy related to defect structures was stored in the GB regions. The GBs in the GB maps are denoted either by red lines corresponding to low-angle GBs (LAGBs) where the misorientation, θ, is 2–15°, or by black lines corresponding to high-angle GBs (HAGBs) with $\theta > 15°$. The IPF and GB maps exhibit inhomogeneous microstructures including fine equiaxed grains and large elongated grains. These maps indicate the development of subgrains within elongated grains, isolated with LAGBs. Thus, the microstructure is in the process of evolving to equiaxed grains isolated with HAGBs. The average grain/cell size of the UFG copper was measured as 360 nm.

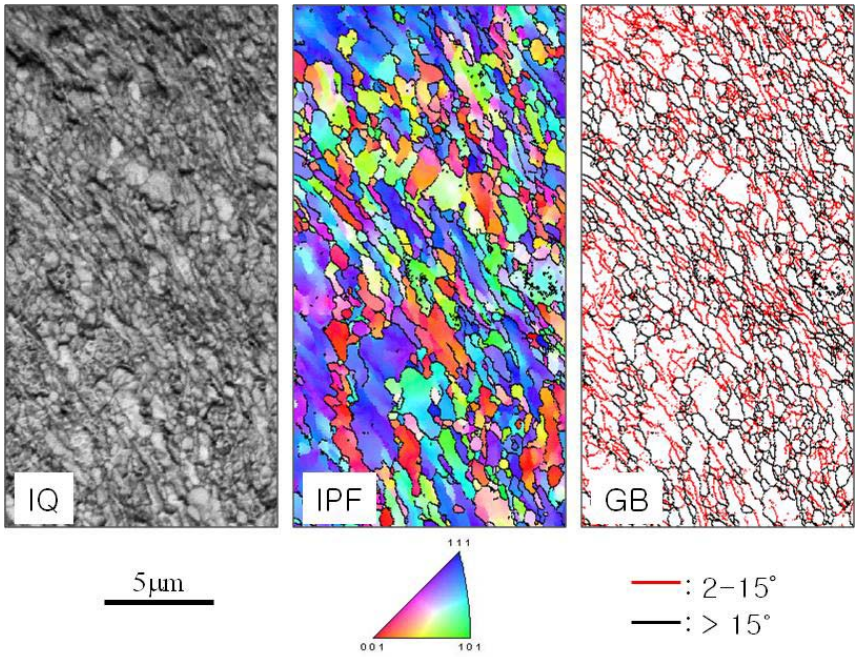

Figure 4. The OIM orientation and GB maps for copper after ECAP through 8 passes.

Figure 5 shows the characteristics of the GBs plotted as a function of the misorientation angle, indicating that UFG copper is weakly bimodal with peaks at low and high misorientation angles. Excessive LAGBs remained because of the continuous introduction of dislocations in each ECAP processing pass. The fraction of HAGBs of UFG copper was approximately 47%.

Figure 6 shows the S-N diagrams of smooth specimens (without a hole) and drilled specimens of UFG copper. The diagram of coarse grained copper smooth specimens is shown by a dashed line alone. For UFG copper examined under stress controlled testing,

the enhancement in fatigue life is obvious. The degree of enhancement is sharply increased with increasing stress amplitude. In the long-life field in excess of $N = 5x10^7$ cycles, however, the fatigue life to failure of UFG tends to coincide with that of coarse grained copper. On the other hand, the fatigue life of drilled specimens is about half of smooth ones, roughly speaking the half a fatigue life was spent to initiate 0.1 mm length cracks in smooth specimens.

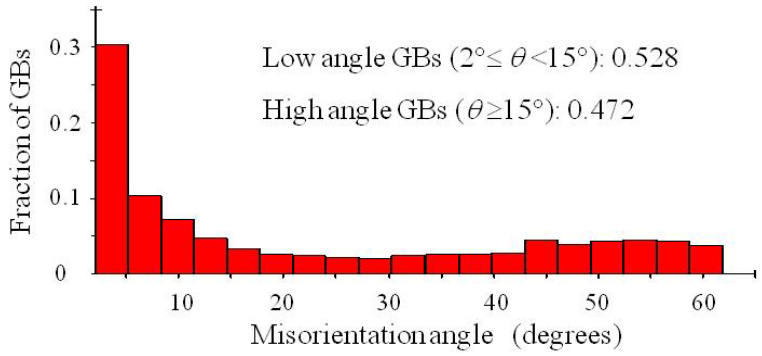

Figure 5. Histograms of the misorientation angles after 8 passes of ECAP.

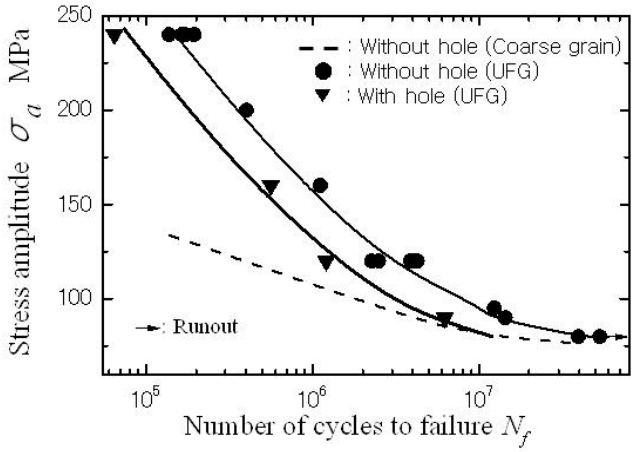

Figure 6. S-N curves

Figures 7a and 7b show the crack growth paths under constant stress amplitudes. At σ_a = 240 MPa, the crack that initiated from the hole created a 45° incline to the loading axis. The 45° inclined crack growth direction has been commonly observed in the ZX-plane of LCF UFG metals [8,10,11]. Regarding the crack propagating under σ_a = 90 MPa, however, the macroscale growth direction was perpendicular to the loading axis. The crack propagated in a zigzag manner at the microscale. The degree of zigzag growth gradually increased with crack length.

To clarify the difference in crack growth mechanism between the high- and low-stress amplitudes, two-step fatigue stress tests were conducted, i.e., after the formation of a crack with an arbitrary length at the first stress amplitude (σ_{a1}), the crack continued

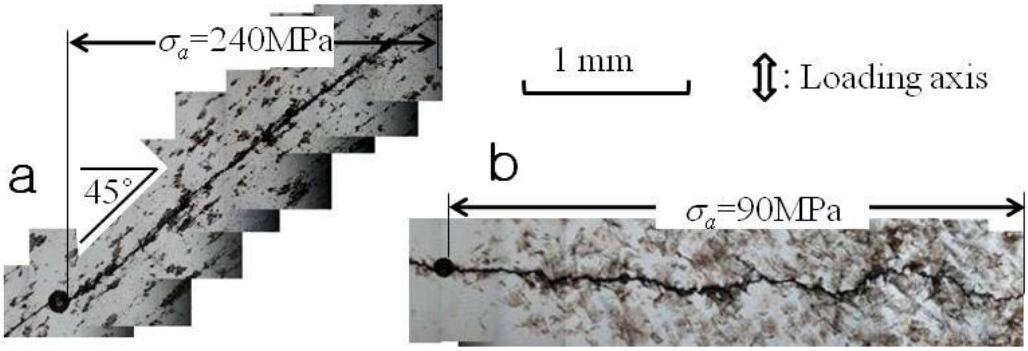

Figure 7. Crack growth paths under constant stress amplitudes; (a) σ_a = 240 MPa, (b) σ_a = 90 MPa.

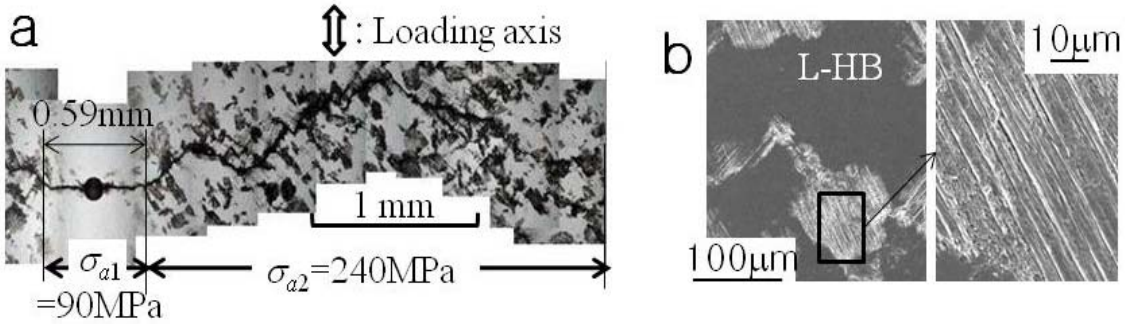

Figure 8. Morphological features around crack path under low-to-high block stressing; (a) crack growth paths, (b) SEM micrographs of typical damaged area.

to grow at the second-stress amplitude (σ_{a2}). Figure 8a shows the crack growth paths under low-to-high block (L-HB) stress. The crack grew perpendicular to the loading axis under σ_{a1} = 90 MPa and its length reached an approximate length l = 0.59 mm after 2.2×10^6 repetitions. Under the second stress (σ_{a2} = 240 MPa), although the crack paths on the macroscale were nearly perpendicular to the loading axis, the crack path had many branches and meanderings and showed a drastically large zigzag pattern. Figure 2b shows the fatigue damage of surface about 350 μm apart from the crack path of post-fatigued specimens. Grain coarsening occurred for L-HB stressing and the slip bands developed inside the coarse grains.

Figure 9a shows the crack growth paths under high-to-low block (H-LB) stress. A 0.53-mm-length crack with a growth path at a 45° incline to the loading axis was formed under 5.3×10^4 repetitions of σ_{a1} = 240 MPa. After a stress amplitude change to σ_{a2} = 90 MPa, the crack grew nearly perpendicular to the loading axis, leaving a linear crack path with very small deflections, while the crack path under the constant stress of σ_a = 90 MPa exhibited a comparatively large zigzag pattern. Figure 9b shows the fatigue damage of surface about 300 μm apart from the crack path of post-fatigued specimens.

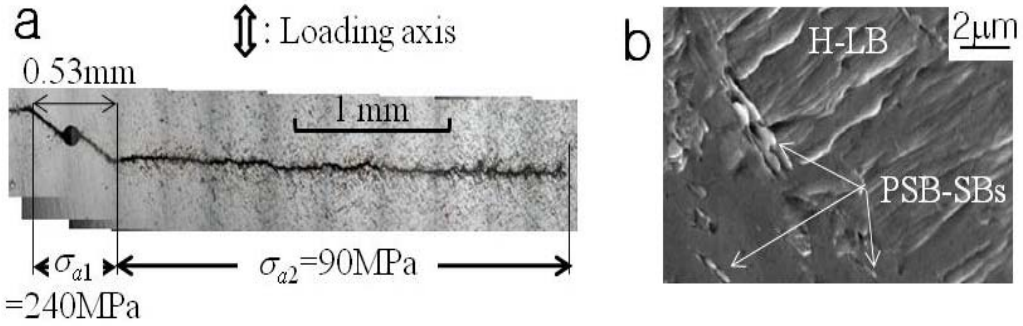

Figure 9. Morphological features around crack path under high-to-low block stressing; (a) crack growth paths, (b) SEM micrographs of typical damaged area.

For the H-LB stressing, persistent slip bands (PSBs) like SBs [26] formed under the high-stress repetitions, and the plate-like protrusions that formed under low-stress amplitude were distributed throughout the fatigued surface. The plate-like protrusions exit the matrix at an incline, forming a terraced field of overlapping plate-like protrusions.

Figure 10 shows the change in surface states around the crack tips just before and after the stress change for L-HB stressing. Figure 10a shows the surface damage just before the stress change, exhibiting a coarsened grain labeled "A" that formed under large repetitions of low-stress amplitude. The grain was accompanied by slip bands. After the stress change (Fig. 10b), a shear crack formed at the major crack tip and grew along the grain boundaries (GBs) of the coarsened grain A. The shear crack stopped propagating after it reached a coarse grain labeled "B." This coarse grain B might be formed under the large first low-stress repetitions, and it became visible by the damaged traces formed under the second high-stress repetitions. It has been reported that the size of the coarsened grains formed by 7,000 cycles of constant stress σ_a = 240 MPa was less than 1 μm, which is equivalent to the PSB-like SB size formed at this stage [27], suggesting that the coarse grain B over 50 μm cannot be formed by 3,000 second-stress cycles. After the stop propagation of the shear crack, the SBs, denoted by "C," were initiated. At 6,000 second-stress cycles, the SB growth ceased and the major crack changed its growth direction, followed by the crack growth with continued SB formation and branching. Meanwhile, several studies on the GBs of UFG copper prepared by severe plastic deformation techniques have seemingly proven the existence of highly non-equilibrium GBs with high energy, excess volume, and long-range stress fields [2,28,29]. Accordingly, diffusion is considerably accelerated in GB regions, where GB sliding can easily occur. Thus, the crack may propagate with the assistance of sliding along the plane of maximum shear stress, showing a straight growth path along the shear direction. Unlike the shear crack growth under the constant stress of σ_a = 240 MPa, the shear crack never continue to grow along its growth direction. This may be attributed to: i) a suppressed sliding result from the lower non-equilibrium states related to the occurrence of patchy distribution of coarse grains over a few tens of micrometers;

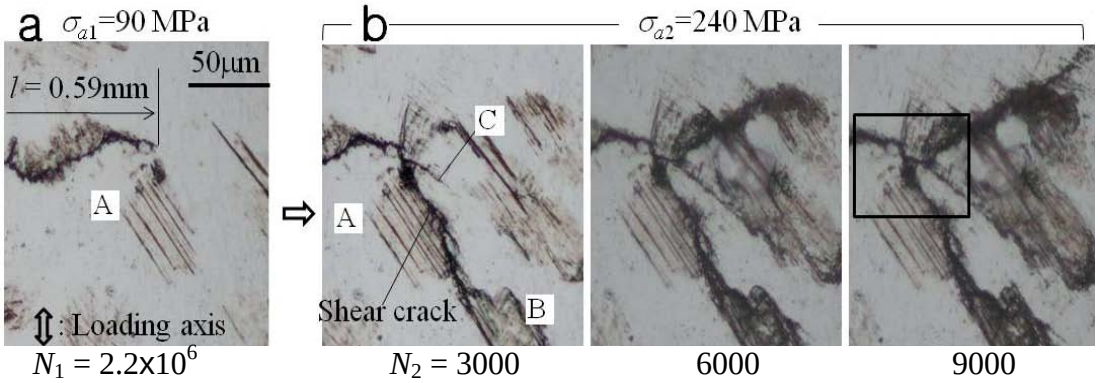

Figure 10. Surface state changes around the crack tip just before and after the stress change for low-to-high block stressing.

ii) arrest of the shear crack growth upon reaching the coarsened grains; and iii) a smaller driving force for the shear crack related to a mismatch of crack face directions between the major and the shear crack (in the constant stressing, the directions of both faces were nearly same, inclined 45° to the loading axis). Consequently, the drastically large zigzag paths were attributed to the crack-branching caused by SB formation, blocking growth at coarse grains and the growth along HAGBs of the coarse grains. It has been shown that fatigue cracks propagate preferentially along HAGBs since they comprise weaker cohesion in their lattice structure [30].

Figure 11 shows the change in surface state around the crack tips just before and after the stress change of the H-LB stressing. Figure 11a shows the surface damage just before the stress change. The crack grew along the plane along an incline of about 45° to the loading axis and the crack path accompanied by a narrow band composed of a large number of fine SBs. The breadth of the band along the crack path was about 35 μm, which was nearly equivalent to the reversible plastic zone size, r_{rp}, that was calculated by assuming a plane stress condition (r_{rp} = 29.8 μm). At 2 × 10^5 cycles of the second stress (Fig. 11b), no newly initiated SBs were observed at the region ahead of

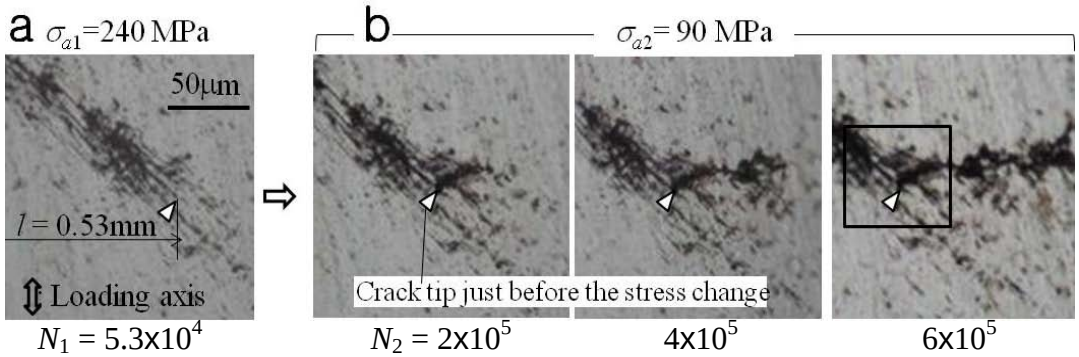

Figure 11. Surface state changes around the crack tip just before and after the stress change for low-to-high block stressing.

the crack tip just before the stress change, as highlighted by an open triangle. Heavily damaged zones were created at the crack tip instead of SBs. The crack grew nearly perpendicular to the loading axis, leaving damaged traces adjacent to the crack path. On the other hand, the growth path under the second stress was comparatively straight compared with that under the constant stress amplitude of σ_a = 90 MPa. Smaller growth path deflection appears to result from the suppression of grain coarsening under the second stress. This suppressed coarsening may relate with the release of non-equilibrium energy due to high-stress preloading.

Figures 12a and 12b show SEM micrographs of highlighted areas shown in Figs. 10b and 11b, respectively. The SEM micrograph for L-HB stressing shows that the shear crack formation commenced at the same time as the stress change. For H-LB stressing, the surface at the crack edges that were formed under high stress was comparatively flat, whereas the surface that formed under low stress had traces of localized plastic deformations, suggesting change in the crack growth mechanism under high and low stresses. In conclusion, the crack at high-stress amplitudes grows along the direction at an incline of 45° to the loading axis because of the sliding induced by the maximum shear stress and the SB decohesion process [31]. At low stress, the crack propagates via the striation formation mechanism, which is associated with crack tip retardation and blunting, because SB formation and decohesion are suppressed under low stresses below a threshold value.

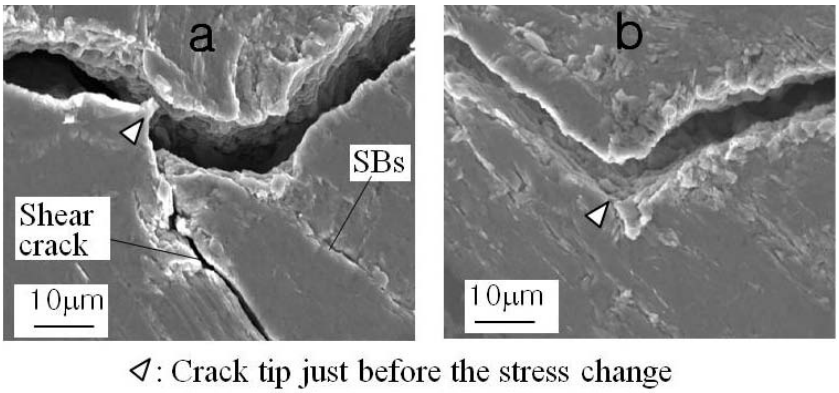

Figure 12. SEM micrographs of the crack paths at the point at which the stress changed; (a) low-to-high block stressing, (b) high-to-low block stressing.

CONCLUSIONS

The main findings of this study can be summarized as follows:
(1) At constant high-stress amplitudes, the crack that initiated from the hole created a 45° incline to the loading axis. The 45° inclined crack growth direction has been commonly observed in the ZX-plane of LCF UFG metals. At constant low-stress amplitudes, however, the macroscale growth direction was perpendicular to the loading

axis, whereas the crack propagated in a zigzag manner at the microscale. The degree of zigzag growth gradually increased with crack length.
(2) The 45° inclined crack growth direction at high stress is result of the sliding induced by the maximum shear stress and the SB decohesion process. At low stress, the crack propagates via the striation formation mechanism.
(3) In the case of low-to-high block stressing, in macroscale the crack growth direction before and after the stress change was nearly perpendicular to the loading axis. On a microscale, however, the degree of zigzag manner in the crack growth drastically increased after the stress change. For high-to-low block stressing, the 45° inclined growth direction under high stress changed to the perpendicular direction under subsequent low stress.
(4) A large number of pre-stressing at low stress amplitudes contributed to the formation of coarsened grains over a few tens of micrometers and a release of high energy in the microstructure, producing a change in crack growth mechanism at subsequent high stress amplitudes. Pre-stressing at high stress amplitudes also released the high energy by forming SBs and coarsened grains less than a few micrometers, but no grain coarsening occurred at subsequent stressing of low amplitudes, giving rise to a linear crack path with very small deflections.

ACKNOLEDGEMENTS

This study was supported by a Grant-in-Aid (23560093) for Scientific Research (C) from the Ministry of Education, Science and Culture of Japan as well as the National Research Foundation of Korea (NRF) grant funded by the Korea government (MEST) (No. 2011-0030801)" and by a grant from Integrated Technology of Industrial Materials funded by the Ministry of Knowledge Economy, Republic of Korea. The authors are very grateful to the members of the Strength of Materials Laboratory of Oita University, for their excellent experimental assistant. Thanks are also extended to the members of Korea Institute of Materials Science, for performing the ECAP processing of our copper rods.

REFERENCES

1. Valiev, R.Z., Islamgaliev, R.K., Alexandrov, I.V. (2000) *Prog. Mater. Sci.* **45**, 103–189.
2. Valiev, R.Z., Kozlov, E.V., Ivanov, Y.F., Lian, J., Nazarov, A.A., Baudelet, B. (1994) *Acta Metall.* **42**, 2467-2475.
3. Agnew, S.R., Weertman, J.R. (1998) *Mater. Sci. Eng.* **A244**, 145.
4. Agnew, S.R., Vinogradov, A.Yu., Hashimoto, S., Weertman, J.R. (1999) *J. Electronic Mater.* **28**, 1038-1044.
5. Vinogradov, A., Hashimoto, S. (2001) *Mater. Trans.* **42**, 74-84.
6. Höppel, H.W., Zhou, Z.M., Mughrabi, H., Valiev, R.Z. (2002) *Philos. Mag.* **A87**, 1781-1794.

7. Mughrabi, H., Höppel, H.W., Kautz, M. (2004) *Scripta Mater.* **51**, 807-812.
8. Maier, H.J., Gabor, P., Karaman, I. (2005) *Mater. Sci. Eng.* **A410**, 457-461.
9. Goto, M., Han, S.Z., Yakushiji, T., Lim, C.Y., Kim, S.S. (2006) *Scripta Mater.* **54**, 2101-2106.
10. Zhang, Z.F., Wu, D.S., Li, Y.J., Liu, S.M., Wang, Z.G., (2005) *Mater. Sci. Eng.* **A412**, 279-286.
11. Xu, C., Wang, Q., Zheng, M., Li,J., Huang, M., Jia, Q., Zhu, J., Kunz, L., Buksa,M. (2008) *Mater. Sci. Eng.* **A475**, 249-256.
12. Fang, D., Zhang, P., Duan, Q., Wu, S., Zhang, Z., Li, J., Zhao, N. (2007) *Advanced Eng. Mater.* **9,** 860-866.
13. Vinogradov, A., Nagasaki, S. Patlan, V., Kitagawa, K., Kawazoe, M. (1999) *NanoStruct. Mater.* **11,** 925-934.
14. Chung, C.S., Kim, J.K., Kim, H.K., Kim, W.J. (2002) *Mater. Sci. Eng.* **A337**, 39-44.
15. Pao, P.S., Jones, H.N., Cheng, S.F., Feng, C.R. (2005) *Inter. J. Fatigue* **27**, 1164-1169.
16. Cavaliere, P. (2009) *Inter. J. Fatigue* **31**, 1476-1489.
17. Collini, L. (2010) *Eng. Fract. Mech.* **77**, 1001-1011.
18. Kim, H.K., Choi, M.-I., Chung, C.S., Shin, D.H. (2003) *Mater. Sci. Eng.* **A340**, 243-250.
19. Hanlon, T., Tabachnikova, E.D., Suresh, S. (2005) *Inter. J. Fatigue* **27**, 1147-1158.
20. Meyer, L.W., Sommer, K., Halle, T., Hockauf, M. (2008) *J. Mater. Sci.* **43**, 7426-7431.
21. Niendorf, T., Rubitschek, F., Maier, H.J., Canadinc, D., Karaman, I. (2010) *J. Mater. Sci.* **45**, 4812-4821.
22. Goto, M., Ando, Y., Han, S.Z., Kim, S.S., Kawagoishi, N., Euh, K. (2010) *Eng. Fract. Mech.* **77**, 1914-1925.
23. Goto, M., Han, S.Z., Euh, K., Kang, J.-H., Kim, S.S., Kawagoishi, N. (2010) *Acta Mater.* **58**, 6294-6305.
24. Goto,M., Kamil, K., Han, S.Z., Euh, K., Kang, J.-H., Kim, S.S., Yokoho, Y. (2012) *Inter. J. Fatigue* (In press), DOI: 10.1016/j.ijfatigue.2012.02.020.
25. Iwahashi, Y., Wang, J., Horita, Z., Nemoto, M., Langdon, T.G. (1995) *Scripta Mater.* **35**, 143-146.
26. Wu, S.D., Wang, Z.G., Jiang, C.B., Li, G.Y., Alexandrov, I.V., Valiev, R.Z. (2003) *Scripta Mater.* **48**, 1605-1609.
27. Goto, M., Han, S.Z., Yakushiji, T., Kim, S.S., Lim, C.Y. (2008) *Inter. J. Fatigue* **30**, 1333-1344.
28. Valiev, R.Z. (1995) *NanoStruct. Mater.* **6**, 73-82.
29. Goto, M., Han, S.Z., Kim, S.S., Kawagoishi, N., Lim, C.Y. (2007) *Scripta Mater.* **57**, 293-296.
30. Zhang, Z.F., Wang, Z.G. (2000) *Mater. Sci. Eng.* **A284**, 285-291.
31. Zhang, J.Z. (2000) *Eng. Fract. Mech.* **65**, 665-681.